



Quantum Inspire Starmon-7 Fact Sheet

M. Samiotis, G.R. Di Carlo, and L. DiCarlo

QuTech and Kavli Institute of Nanoscience, Delft University of Technology, P.O. Box 5046, 2600 GA Delft, The Netherlands

(Dated: February 5, 2025)

This fact sheet provides further information on the Starmon-7 superconducting backend of Quantum Inspire, including the quantum processor layout, cryogenic wiring, control electronics, quantum operations, and reported metrics.

I. QUANTUM PROCESSOR

Starmon-7 is a superconducting quantum processor based on circuit quantum electrodynamics [1, 2]. It consists of seven transmon qubits [3] (labelled Q_0 to Q_6) in the configuration shown in Fig. 1. This configuration is best described as two rhombi with qubits at each vertex and dedicated bus resonators on each edge. The two rhombi have a common vertex (Q_3).

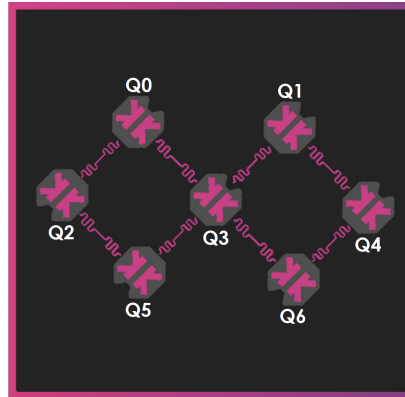


FIG. 1. Simple logo for Starmon-7 showing its connectivity graph.

A schematic of the $8 \text{ mm} \times 8 \text{ mm}$ chip is shown in Fig. 2. Eight dedicated bus resonators connect every pair of nearest-neighbor qubits, enabling native two-qubit controlled- Z (CZ) gates between them. Each transmon is also connected to a microwave-control line for single-qubit gating, a flux-control line for two-qubit gating, and a dispersively-coupled resonator for readout. Every readout resonator has an accompanying Purcell filter [4]. The readout resonator structures for qubits Q_0 and Q_2 couple to one feedline, and those of all other qubits to another. The unique frequencies of the readout structures allow simultaneous, independent qubit readout by frequency multiplexing. The 7-port connectivity of these transmons gives them a characteristic star shape and hence the nickname *Starmon* [5]. All inputs and outputs of the device are connected to a Cu printed circuit board using Al wirebonds, as shown in Fig. 3.

II. DILUTION REFRIGERATOR WIRING

Starmon-7 is cooled to 19 mK in a [Leiden Cryogenics](#) Leiden Cryogenics CF-650 $^3\text{He}/^4\text{He}$ dilution refrigerator. Figure 4 shows a photographic image of the inside of the dilution refrigerator. A detailed diagram of the wiring of readout, microwave-control, and flux-control lines inside the refrigerator is shown in Fig. 5. The status of the dilution refrigerator can be followed in real time via this [link](#).

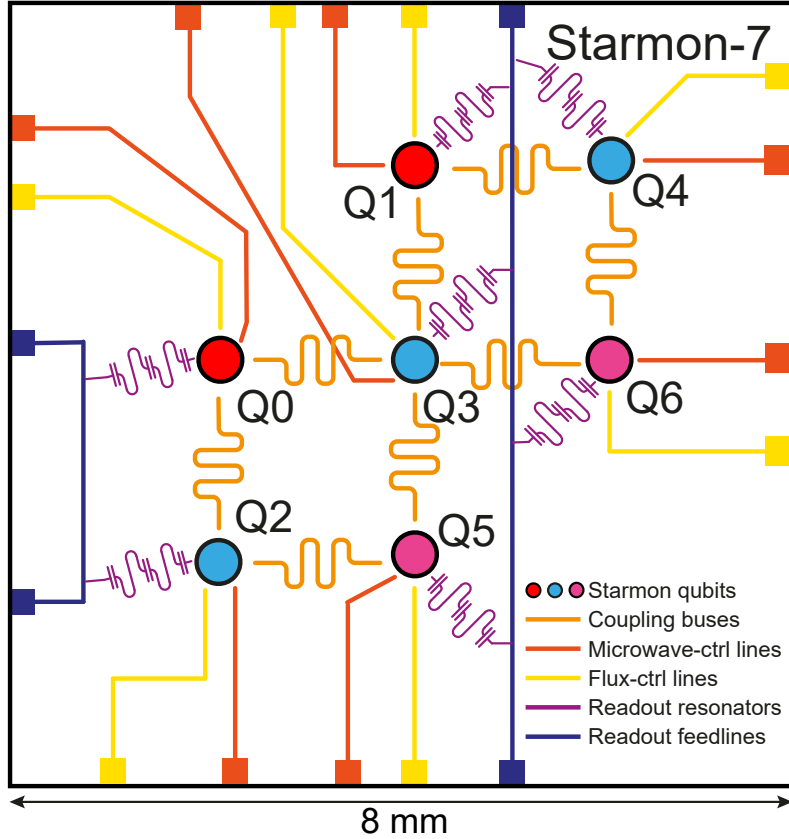


FIG. 2. Schematic diagram of the Starmon-7 quantum processor. The transmons are represented as circles, with color indicating high-frequency (red), mid-frequency (blue), and low-frequency (pink) transmons. The processor architecture follows Ref. [5].

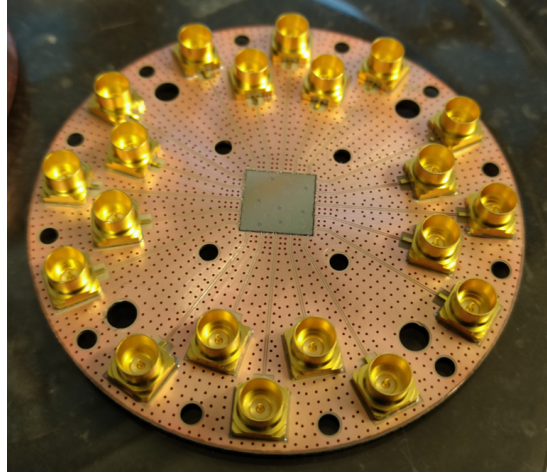


FIG. 3. Optical image of a similar device mounted to its Cu printed circuit board.

III. CONTROL ELECTRONICS

The Starmon-7 processor is controlled using a room-temperature electronics stack. This stack combines special-purpose QuTech-built and commercially available electronics (mostly [Zurich Instruments](#)), as shown in the schematic in Fig. 6.

The QuTech Central Controller is an all-digital instrument whose primary function is to orchestrate the action of all analog control and readout instruments. This sequencer can generate up to 50 million sequences per instrument

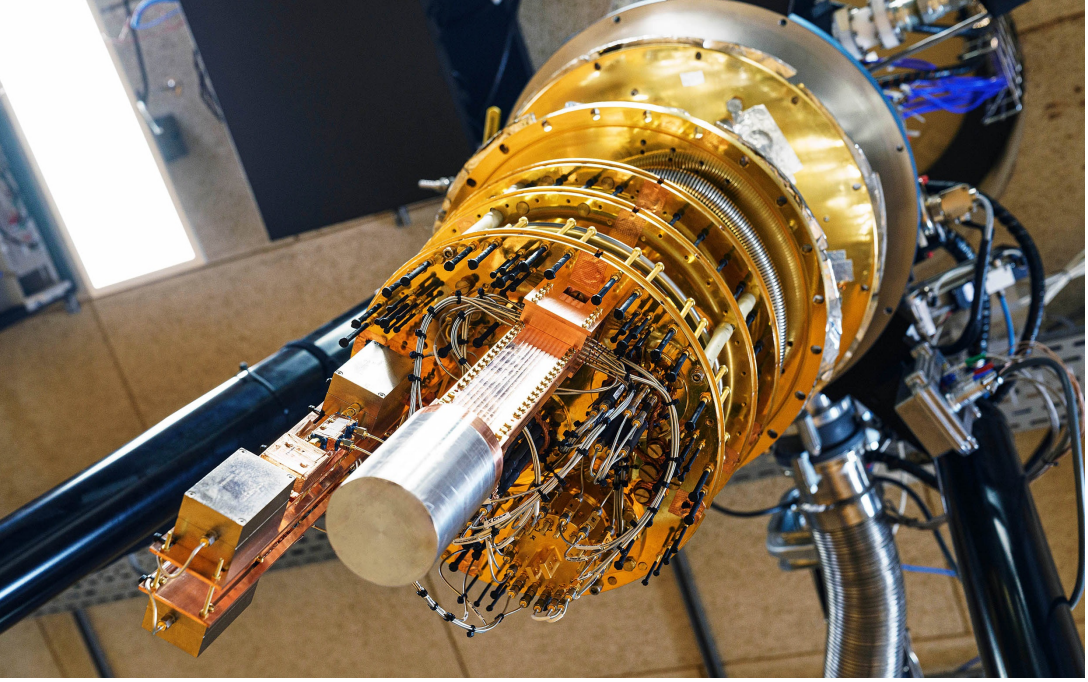


FIG. 4. Photograph of the Leiden Cryogenics dilution refrigerator housing Starmon-7.

per second. It makes use of a distributed architecture to control up to 12 analog instruments per rack, ensuring extensibility to Starmon-17 (such a system is currently used for research purposes in DiCarlo lab). It achieves this while guaranteeing timing determinism.

The Zurich Instruments High-Density Arbitrary Waveform Generator (HDAWG8) is an eight-channel arbitrary waveform generator (AWG) used to produce both the flux pulses required for two-qubit gates and the envelopes of microwave-frequency pulses used for single-qubit gates. The HDAWG8 has real-time filtering capabilities that we use to correct the linear-dynamical distortions in the flux-control lines [6]. Starmon-7 makes use of 3 HDAWGs in total (one for flux control, and two for microwave control).

The Zurich Instruments Ultra-High Frequency Quantum Analyzer (UHFQA) is an all-in-one two-channel AWG and two-channel digitizer used to perform readout. The AWG produces the envelopes of microwave readout pulses injected to a feedline. The digitizer performs demodulation and weighted integration of the feedline output signal (after amplification and frequency down-conversion) and thresholds, producing a one-bit outcome for each qubit measured. Starmon-7 makes use of two UHFQAs, one per feedline.

The Zurich Instrument Super-High Frequency Parametric Pump Controller (SHFPPC) is used to provide the pump tone for each travelling-wave parametric amplifier (TWPAs), and also to interferometrically null the pump at the input to the readout down-conversion mixer.

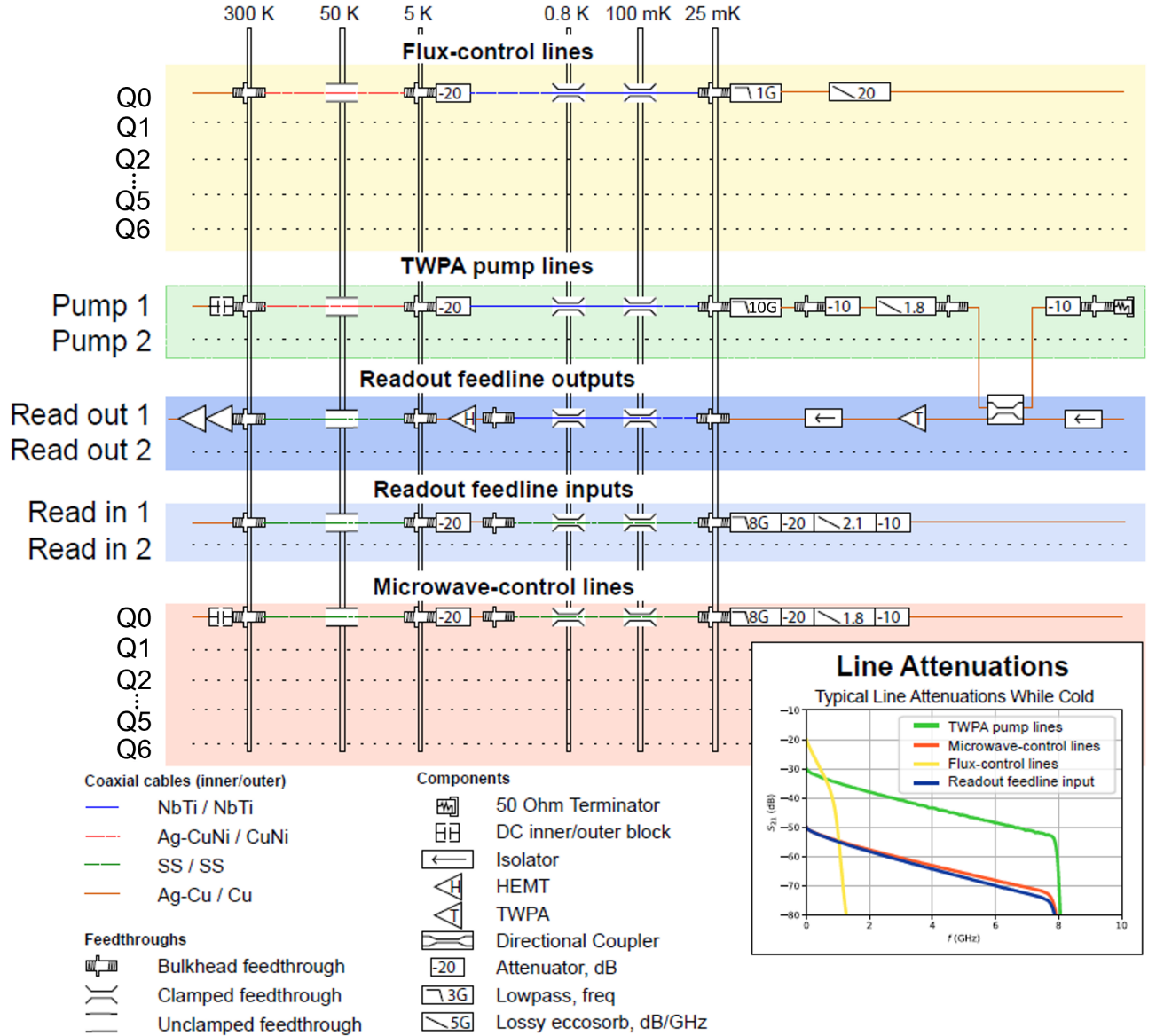


FIG. 5. Diagram the cryogenic cabling used in Starmon-7.

IV. LEGACY

Seven-transmon devices of nearly identical design, the exact control stack, and under-the-hood data-acquisition platform have been previously used in the DiCarlo lab in QuTech for NISQ applications and developments toward quantum error correction. For further reference, we invite interested readers to consult the following scientific publications:

- Realization of the Sudden Net-Zero CZ gate [7].
- Quantum simulation: preparation of thermofield double states [8].
- Quantum neural networks using a repeat-until-success scheme [9].
- Quantum error detection using the distance-2 surface code [10].

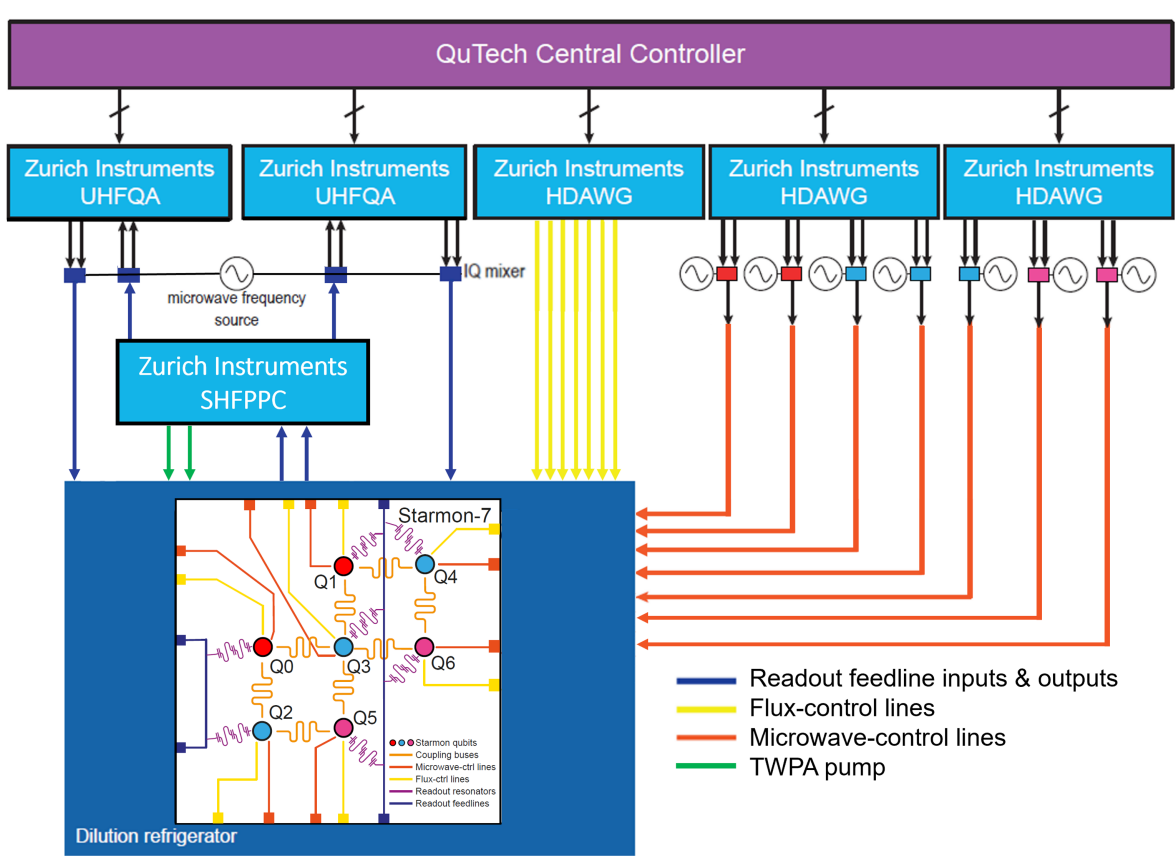


FIG. 6. Schematic diagram of the key instruments in the room-temperature electronics control stack of Starmon-7.

V. COMPARISON TO PREVIOUS STARMON BACKENDS

Compared to Starmon-5, Starmon-7 has the following improvements:

- Increased number of available qubits, from 5 to 7.
- Increased number of available nearest-neighbor qubit pairs, from 4 to 8.
- Faster readout time, from 2 to 1 μ s, made possible by post-fabrication trimming of readout resonator and Purcell-filter frequencies using the *Shoelacing* technique [11].

VI. QUBIT OPERATIONS

Single-qubit gates: The native single-qubit gates of Starmon-7 are I , the longitudinal gates Z , S , S^\dagger , T , and T^\dagger , and the transversal gates X , $X90$, $mX90$, Y , $Y90$, $mY90$, x -axis rotations $R_x(\theta)$, and y -axis rotations $R_y(\theta)$, with θ any multiple of $\pi/28$. Users can specify arbitrary θ , but the compiler quantizes to the nearest multiple of $\pi/28$. The above longitudinal gates are implemented using virtual Z gates (i.e., updating the phase of the reference oscillator for each qubit). The transversal gates are implemented as DRAG pulses [12, 13], with their characteristic gaussian and derivative-of-gaussian envelopes. All native single-qubit gates complete within 20 ns. This includes I , which amounts to 20 ns of idling.

Starmon-7 supports other single-qubit gates non-natively. These are:

- H , realized as $R_x(\pi)R_y(\pi/2)$,
- $R_z(\theta)$, realized as $R_y(-\pi/2)R_x(\theta)R_y(\pi/2)$.

Two-qubit gates: The only native two-qubit gate in Starmon-7 is the CZ gate between nearest neighbors (8 pairs in total). The realization of this gate exploits the flux-controlled interaction between computational states $|11\rangle$ and the non-computational state $|02\rangle$, where 2 refers to the second-excited state of the higher-frequency transmon in the pair [14]. We use the Sudden Net-Zero flux pulse [7] to perform the CZ gate. All CZ gates complete within 60 ns.

Readout: Native measurement in Starmon-7 is in the computational (Z basis). Measurement is performed with a frequency-multiplexed pulsed measurement of feedline transmission at the frequencies of the readout-Purcell-filter pairs of specified transmons. Readout excitation pulses vary from 250 to 600 ns duration. The response at each frequency is demodulated and integrated (using optimal weight functions [15]) over 0.95 μ s. The total readout duration, including photon depletion, is 1 μ s for all qubits. Starmon-7 supports measurement in the X and Y bases non-natively, realized using pre- and post-rotations.

VII. REPORTED METRICS

Key performance characteristics are extracted with every calibration of Starmon-7. These characteristics are kept up to date at this [link](#). Below we provide a description of the extraction method for each characteristic.

Qubit relaxation and dephasing times: The relaxation time T_1 and the echo dephasing time T_2^{echo} for each qubit are extracted from standard sliding- π pulse and Hahn-echo experiments, respectively [16].

Single-qubit gate fidelity F_{1Q} : We perform single-qubit Clifford randomized benchmarking (RB) to extract an average error per single-qubit Clifford gate. Taking into account that 1.875 native gates are required on average per Clifford gate, we then extract the average error per native single-qubit gate [17].

Two-qubit gate fidelity F_{2Q} : We perform interleaved RB [18] to extract an average error for each CZ gate [19]. We perform now standard modifications [19] to interleaved RB in order to also quantify leakage L_1 .

Initialization fidelity F_{INIT} : We obtain a histogram [20] of the analog output of single-shot readout with the qubit initialized (ideally in $|0\rangle$). We perform a double-gaussian fit to this histogram and associate the dominant (weaker) gaussian to the analog readout for qubit in $|0\rangle$ ($|1\rangle$). The initialization fidelity is given by the ratio of the area of the dominant gaussian to the total area of the double gaussian.

Readout fidelity $F_{\text{R/O}}$: We perform single-shot readout experiments to determine the probability $1 - \epsilon_{10}$ of properly declaring measurement outcome 0 when the qubit is prepared in $|0\rangle$ and the probability $1 - \epsilon_{01}$ of properly declaring 1 when prepared in $|1\rangle$, using the optimal 1-bit discretization threshold. We report the average assignment fidelity [21], given by $F_{\text{R/O}} = 1 - (\epsilon_{10} + \epsilon_{01})/2$. The reported value corrects for the calibrated initialization error.

VIII. LIST OF MAJOR CHANGES AND UPGRADES

- **February 6, 2025:** Public release of Starmon-7 via the [Quantum Inspire](#) platform. Included in the release are example Jupyter notebooks and Python utility functions to help users get started using the Software Development Kit (SDK). The files are available [here](#).

IX. TARGETED UPCOMING UPGRADES

- Expansion of the reported performance parameters to include metrics of interest primarily to experts.
- Public release of the dashboard visualizing the time evolution of device performance parameters.
- Further speedup of readout time, from 1 μ s to 800 ns.
- Improving the dephasing time with improved filtering (requires a thermal cycle).

X. REQUESTS FOR ADDITIONAL MATERIALS

For additional technical information regarding the Starmon-7 processor, cryogenic wiring, control electronics, and reported metrics, please contact Marios Samiotis (m.samiotis@tudelft.nl), G. Ruggero Di Carlo (g.r.dicarlo@tudelft.nl), or Leo DiCarlo (l.dicarlo@tudelft.nl). For all other questions, please contact Vivek Sinha (v.sinha@tudelft.nl).

ACKNOWLEDGMENTS

We thank colleagues at the TNO Radar Group and Zurich Instruments for co-developing the control electronics stack used in all Starmon backends to date. This stack was originally developed during the now concluded IARPA-funded LogiQ program (U.S. Army Research Office Grant No. W911NF-16-1-0071). We also thank G. Calusine and W. Oliver for providing the TWPAs at the front end of each readout amplification chain. We acknowledge funding from the Dutch National Growth Funds KAT-1 StartImpulse program, the allowance for Top Consortia for Knowledge and Innovation (TKIs) of the Dutch Ministry of Economic Affairs, the Netherlands Organization for Scientific Research (NWA.1292.19.194 Quantum Inspire), and Intel Corporation. (The views and conclusions contained here are those of the authors and should not be interpreted as necessarily representing the official policies or endorsements, either expressed or implied, of the ODNI, IARPA, or the U.S. Government.)

- [1] A. Blais, R.-S. Huang, A. Wallraff, S. M. Girvin, and R. J. Schoelkopf, *Phys. Rev. A* **69**, 062320 (2004).
- [2] A. Wallraff, D. I. Schuster, A. Blais, L. Frunzio, R.-S. Huang, J. Majer, S. Kumar, S. M. Girvin, and R. J. Schoelkopf, *Nature* **431**, 162 (2004).
- [3] J. A. Schreier, A. A. Houck, J. Koch, D. I. Schuster, B. R. Johnson, J. M. Chow, J. M. Gambetta, J. Majer, L. Frunzio, M. H. Devoret, S. M. Girvin, and R. J. Schoelkopf, *Phys. Rev. B* **77**, 180502(R) (2008).
- [4] J. Heinsoo, C. K. Andersen, A. Remm, S. Krinner, T. Walter, Y. Salathé, S. Gasparinetti, J.-C. Besse, A. Potočnik, A. Wallraff, and C. Eichler, *Phys. Rev. App.* **10**, 034040 (2018).
- [5] R. Versluis, S. Poletto, N. Khammassi, B. Tarasinski, N. Haider, D. J. Michalak, A. Bruno, K. Bertels, and L. DiCarlo, *Phys. Rev. Applied* **8**, 034021 (2017).
- [6] M. A. Rol, L. Ciociaro, F. K. Malinowski, B. M. Tarasinski, R. E. Sagastizabal, C. C. Bultink, Y. Salathe, N. Haandbaek, J. Sedivy, and L. DiCarlo, *App. Phys. Lett.* **116**, 054001 (2020).
- [7] V. Negîrneac, H. Ali, N. Muthusubramanian, F. Battistel, R. Sagastizabal, M. S. Moreira, J. F. Marques, W. J. Vlothuizen, M. Beekman, C. Zachariadis, N. Haider, A. Bruno, and L. DiCarlo, *Phys. Rev. Lett.* **126**, 220502 (2021).
- [8] R. Sagastizabal, S. P. Premaratne, B. A. Klaver, M. A. Rol, V. Negîrneac, M. Moreira, X. Zou, S. Johri, N. Muthusubramanian, M. Beekman, C. Zachariadis, V. P. Ostroukh, N. Haider, A. Bruno, A. Y. Matsuura, and L. DiCarlo, *npj Quantum Inf.* **7**, 130 (2021).
- [9] M. S. Moreira, G. G. Guerreschi, W. Vlothuizen, J. F. Marques, J. van Straten, S. P. Premaratne, X. Zou, H. Ali, , N. Muthusubramanian, C. Zachariadis, J. van Someren, M. Beekman, N. Haider, A. Bruno, C. G. Almudever, A. Y. Matsuura, and L. DiCarlo, *npj Quantum Inf.* **9**, 118 (2023).
- [10] J. F. Marques, B. M. Varbanov, M. S. Moreira, H. Ali, N. Muthusubramanian, C. Zachariadis, F. Battistel, M. Beekman, N. Haider, W. Vlothuizen, A. Bruno, B. M. Terhal, and L. DiCarlo, *Nat. Phys.* **18**, 80 (2022).
- [11] S. Vallés-Sanclemente, S. L. M. van der Meer, M. Finkel, N. Muthusubramanian, M. Beekman, H. Ali, J. F. Marques, C. Zachariadis, H. M. Veen, T. Stavenga, N. Haider, and L. DiCarlo, *Applied Physics Letters* **123**, 034004 (2023).
- [12] F. Motzoi, J. M. Gambetta, P. Rebentrost, and F. K. Wilhelm, *Phys. Rev. Lett.* **103**, 110501 (2009).
- [13] J. M. Chow, L. DiCarlo, J. M. Gambetta, F. Motzoi, L. Frunzio, S. M. Girvin, and R. J. Schoelkopf, *Phys. Rev. A* **82**, 040305 (2010).
- [14] L. DiCarlo, J. M. Chow, J. M. Gambetta, L. S. Bishop, B. R. Johnson, D. I. Schuster, J. Majer, A. Blais, L. Frunzio, S. M. Girvin, and R. J. Schoelkopf, *Nature* **460**, 240 (2009).

- [15] C. C. Bultink, B. Tarasinski, N. Haandbaek, S. Poletto, N. Haider, D. J. Michalak, A. Bruno, and L. DiCarlo, *App. Phys. Lett.* **112**, 092601 (2018).
- [16] P. Krantz, M. Kjaergaard, F. Yan, T. P. Orlando, S. Gustavsson, and W. D. Oliver, *App. Phys. Rev.* **6**, 021318 (2019).
- [17] M. A. Rol, C. C. Bultink, T. E. O'Brien, S. R. de Jong, L. S. Theis, X. Fu, F. Luthi, R. F. L. Vermeulen, J. C. de Sterke, A. Bruno, D. Deurloo, R. N. Schouten, F. K. Wilhelm, and L. DiCarlo, *Phys. Rev. Applied* **7**, 041001 (2017).
- [18] E. Magesan, J. M. Gambetta, B. R. Johnson, C. A. Ryan, J. M. Chow, S. T. Merkel, M. P. da Silva, G. A. Keefe, M. B. Rothwell, T. A. Ohki, M. B. Ketchen, and M. Steffen, *Phys. Rev. Lett.* **109**, 080505 (2012).
- [19] C. J. Wood and J. M. Gambetta, *Phys. Rev. A* **97**, 032306 (2018).
- [20] D. Ristè, J. G. van Leeuwen, H.-S. Ku, K. W. Lehnert, and L. DiCarlo, *Phys. Rev. Lett.* **109**, 050507 (2012).
- [21] C. C. Bultink, M. A. Rol, T. E. O'Brien, X. Fu, B. C. S. Dikken, C. Dickel, R. F. L. Vermeulen, J. C. de Sterke, A. Bruno, R. N. Schouten, and L. DiCarlo, *Phys. Rev. App.* **6**, 034008 (2016).